

NORMALIZATION OF LIDAR INTENSITY DATA BASED ON RANGE AND SURFACE INCIDENCE ANGLE

B. Jutzi, H. Gross

Institute of Photogrammetry and Remote Sensing, Universität Karlsruhe, Kaiserstr. 12, 76128 Karlsruhe, Germany
boris.jutzi@ipf.uni-karlsruhe.de

FGAN-FOM, Research Institute for Optronics and Pattern Recognition, Gutleuthausstraße 1, 76275 Ettlingen, Germany
gross@fom.fgan.de

KEY WORDS: Full-waveform, intensity, normalization, Lambertian law, Phong model, diffuse, specular, reflectance.

ABSTRACT:

The analysis of airborne laser scanner data to extract surface features is of great interest in photogrammetric research. Especially for applications based on airborne measurements, where the intensity is crucial (e.g. for segmentation, classification or visualization purposes), a normalization considering the beam divergence, the incidence angle and the atmospheric attenuation is required. Our investigations show that the same material of a surface (e.g. gabled roof) yields to different measured values for the intensity. These values are strongly correlated to the incidence angle of the laser beam on the surface. Therefore the intensity value is improved with the incidence angle derived by the sensor and object position as well as its surface orientation. The surface orientation is estimated by the eigenvectors of the covariance matrix including all object points inside a close environment. Further the atmospheric attenuation is estimated. The adaptation of vegetation areas is disregarded in this study. After these improvements the intensity does no longer depend on the incidence angle but may be influenced by the material of the object surface only. For surface modelling the Phong model is introduced, considering diffuse and specular backscattering characteristics of the surface. A measurement campaign was carried out to investigate the influences of the incidence angle on the measured intensity. By considering the incidence angle and the distance between sensor and object the laser data captured from different flight paths (data stripes) can be successfully fused. In our experiments it could be shown that the radiometric normalization of the intensity for the investigated areas are improved.

1. INTRODUCTION

The processing of laser scanner data for the automatic generation of 3d models is of great interest (Brenner et al., 2001; Geibel & Stilla, 2000). Spaceborne, airborne as well as terrestrial laser scanner sensors allow a direct and illumination-independent measurement from 3d objects in a fast, contact free and accurate way (Shan & Toth, 2008). Beside basic range measurements the current commercial airborne laser scanner (ALS) developments allow to record the amplitude or the waveform of the backscattered laser pulse. For this purpose laser scanner systems like OPTECH ALTM 3100, TOPEYE MK II, and TOPOSYS HARRIER 56 can be used. The latter system is based on the RIEGL LMS-Q560. More and more waveform capturing scanners are available at the moment, e.g. RIEGL one of the leading companies for laser scanners already offers several scanners (LMS-Q560, LMS-Q680, and VQ-480).

The measured waveform itself includes information about different features like range, elevation variations, and reflectance of the illuminated surface based on the inclination between the divergent laser beam and object plane. To interpret the received waveform of the backscattered laser pulse a fundamental understanding of the physical background of pulse propagation and surface interaction is important. The waveform of each laser pulse can be described by a distributed series of range values combined with amplitude values. Depending on the shape of the waveform it can be approximated by one or more parameterized Gaussian curves (Hofton et al., 2000; Persson et al., 2005; Wagner et al., 2006). Due to this approximation the temporal position, width and amplitude caused by the object surfaces are estimated (Jutzi & Stilla, 2006). With these parameters the geometry and the reflectance of the illuminated surface can be investigated. The material reflectance features from the measured data mainly depends on the incidence angle of the beam on the surface, the surface properties and the laser wavelength (Jelalian, 1992).

In the terminology of laser scanning the reflectance is widely used as synonym for the amplitude or energy, where the energy of each pulse is the integral over its waveform. For a Gaussian pulse this can be simplified and approximated by the product of amplitude and width. Beside this the term intensity is used for the amplitude or energy. Various studies about surface reflectance and the intensity calibration have been published in the literature:

- Briese et al. (2008) proposed to use natural surfaces with known backscattering characteristic measured by a reflectometer for radiometric calibration of full-waveform data.
- Höfle & Pfeifer (2007) showed a data and a model-driven method for correcting the intensity for specific influences. The corrected intensity is successfully used to generate intensity images with lower systematic errors.
- Kaasalainen et al. (2007) suggested to use in the laboratory measured reference targets for calibrating the intensity values derived by airborne laser scanner sensors.
- Katzenbeisser (2003) introduced for flat surfaces that the measured intensity provide a reasonable mean for the reflectance, if the measured intensity is corrected by the known distance.
- Kukko et al. (2007) measured for various urban materials the dependency of the intensity from the incidence angle.
- Pfeifer et al. (2007) studied the influence on the intensity for surfaces with varying incidence angles, known reflectance and scattering characteristics. It is shown that the range dependent inverse-square model might be insufficient to estimate the accurate intensity.
- Reshetyuk (2006) investigated for various materials the surface reflectance and its influences on the measured range and intensity.

- Wagner et al. (2008) gives a review on their proposed calibration procedure and scattering model concerning the cross section and backscattering parameter of an object with diffuse (Lambertian) surface characteristic.

Especially for segmentation, classification or visualization purposes an intensity normalization of the measurements derived by an airborne laser scanner is of great interest. Obviously the variation of the incidence angle increases if data from several flights with different paths (flight stripes) are fused. Further the atmospheric conditions can change slightly while the measurement is carried out or change considerably if multi-temporal data is gained. For these reasons the incidence angle and the atmospheric attenuation has to be taken in account to normalize the intensity.

To give an example for the dependency of the intensity from the incidence angle an RGB-image together with the corresponding intensity values from two different flights are visualized in Figure 1. The viewing direction of the sensor system is depicted by a black arrow. The area of interest is the gabled roof. Obviously the roof area orientated towards the sensor systems delivers higher intensity values, while the turn away roof area delivers significant smaller intensity values.

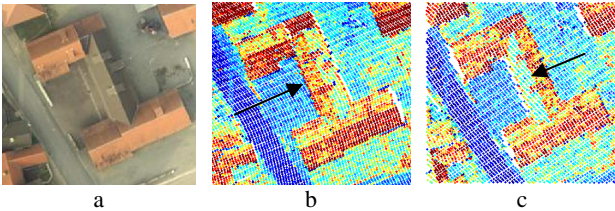


Figure 1: Dependency of the intensity from the incidence angle:
a) RGB image,
b) Intensity values of flight 3 measured from left,
c) Intensity values of flight 4 measured from right.

These from the laser data estimated intensity values are strongly correlated to the incidence angle of the laser beam on the surface. Therefore we propose to normalize the value of the intensity by considering the incidence angle derived by the sensor and object position as well as its surface orientation. We estimate the orientation by utilizing the available data concerning the neighbourhood of each measured laser point. To increase the accuracy of the intensity estimation the atmospheric attenuation parameter of the particular measurement campaign is determined empirically in advance. The non-linear effects on the measured intensity induced by electronically receiver components are not investigated in this work, but these might have influences on the measurement as well.

In Section 2 the physical constraints of the Lambertian and Phong surface model, a data-driven parameter estimation approach, and the methodology for calculation of the normal vectors of the surfaces based on the covariance matrix with the derived incidence angle are introduced. The gathered data set is introduced in Section 3. In Section 4 homogenous test regions are selected for the assessment of the normalization. The results for the data-driven parameter estimation, of the normalized intensity of the investigated planes are shown and evaluated. Finally the derived results are discussed.

2. METHODOLOGY

Concerning full-waveform laser data for each single beam the total number of detected backscattered pulses is known and is assigned to the corresponding echoes. Each echo is described

by a point with its 3d coordinate, signal amplitude a , and signal width w at full-width-at-half-maximum derived from the Gaussian approximation. Additionally the 3d coordinate of the sensor position is available.

The shape of the received waveform depends on the illuminated surface area, especially on the material, reflectance of the surface and the inclination angle between the surface normal and the laser beam direction. The typical surface attributes which can be extracted from a waveform are range, elevation variation, and reflectance corresponding to the waveform features: time, width and amplitude.

The intensity (energy) is estimated by the width multiplied with the amplitude of the Gaussian approximation and modified by the range between sensor and object with respect to the extinction by the atmosphere and the divergence of the laser beam. It describes the reflectance influenced by geometry and material of the object at this point. For each particular echo caused by partially illuminated object surfaces an individual intensity value is received.

2.1 Laser beam, transmission and surface model

The received energy $E_r = c \cdot a \cdot w$ of a monostatic laser scanner system can be calculated by the amplitude and width of the received signal approximation. The factor c is constant and has therefore no influence for our consideration. Considering an energy balance it depends on the transmitted energy E_t , the distance R to the object surface, and the incidence angle ϑ , which is given by the angle between the transmitter direction and the surface normal vector

$$E_r = E_t \cdot C_t \cdot C_r \cdot R^{-2} \cdot e^{-2\alpha R} \cdot \cos(\vartheta) \cdot f(c_s), \quad (1)$$

where C_t and C_r are constant terms of the transmitter and the receiver (Kamermann, 1993; Pfeifer et al., 2007).

The atmospheric attenuation along the way from the transmitter to the object and return to the receiver is $e^{-2\alpha R}$. Let $f(c_s)$ entail all other influences like surface material and local surface geometry. This formula is valid for objects with larger size than the footprint of the laser beam. All constant terms may be ignored because only the received intensity is of interest. If the received amplitude and width of the signal is given a range corrected intensity can be calculated

$$I_R = C_1 \cdot a \cdot w \cdot R^2 \cdot e^{2\alpha R}, \quad (2)$$

where C_1 may be any arbitrary constant. This intensity I_R does not dependent on the distance R anymore. I_R is influenced by the material properties and the incidence angle. Nonlinear effects of the photodiode are not considered by this assumption.

For all points with high planarity the measured intensity is normalized by $I = I_R / \cos(\vartheta)$ considering the incidence angle. The illumination direction \vec{e}_t is calculated from the sensor to the object position. The normal vector of an object surface is determined by the evaluation of the covariance matrix, cf. Section 2.4, with respect to the smallest eigenvalue λ_3 and its eigenvector \vec{e}_3 . With this normalized vectors the required divisor is calculate by $\cos(\vartheta) = |\vec{e}_t \circ \vec{e}_3|$.

With this framework the radiometric calibration of the intensity due to atmospheric influences and surface orientation is possible. Then the normalized intensity I depends on the used wavelength and on the material properties only. The influence of speckle effects is neglected.

2.2 Data-driven parameter estimation

To adapt the dependency of the intensity from the object distance, atmospheric attenuation, and incidence angle the intensity in Formula 2 is generalized by

$$I_A = IR^a e^{2bR} \cos^c(\vartheta) e^d \quad (3)$$

where I is the measured intensity, R the distance between the sensor and the object, ϑ the incidence angle and a, b, c, d constant parameters. Herein describes a the beam divergence. The exponent $2bR$ concerns the attenuation by the two way propagation of the laser beam. The term c models the type of reflectivity and d normalizes the whole value to be equal with 1. Inside a homogenous region the adapted intensity should be nearly constant. Therefore the unknown parameters have to be determined resulting in the smallest variation inside homogenous areas. Therefore it can be postulated that

$$I_{A,i} = I_i R_i^a e^{2bR_i} \cos^c(\vartheta_i) e^d = 1 + \varepsilon_i \quad (4)$$

where ε_i marks the error of the i -th point of the point cloud of the considered region. This can be realized by the factor e^d . After logarithm reformulation the linear regression problem is given by

$$\sum_{i \in \text{region}} \left(\ln(I_i) + a \ln(R_i) + 2bR_i + c \ln(\cos(\vartheta_i)) + d \right)^2 \rightarrow \text{Min} \quad (5)$$

which results in a system of linear equations for the unknown parameters. Considering the beam divergence of the laser beam the first unknown $a = 2$ can be set. This assumption is valid for object surfaces larger than the beam footprint. After calculation of the attenuation parameter b and the improvisational surface reflectance adaptation parameter c the last unknown is given by

$$d = -\text{mean}_{i \in \text{region}} \left(\ln \left(IR^a e^{2bR} \cos^c(\vartheta) \right) \right). \quad (6)$$

2.3 Extended surface model for diffuse and specular material reflectance

To enhance the above mention Lambertian surface model the empirical Phong surface model (Phong, 1975) is introduced. Besides the diffuse surface scattering the proposed Phong model can handle as well specular surface characteristics. The general formula is given by

$$I_{out} = I_a k_a + I_{in} \left[k_d \cos(\vartheta) + k_s \cos^n(2\vartheta) \right]. \quad (7)$$

Ignoring the ambient lightning ($k_a = 0$) and considering $k_a + k_d + k_s = 1$ for the diffuse reflectance parameter $k_d = 1 - k_s$ is derived. The remaining parameters are the weighting factors for the diffuse and specular part of the reflection. The adaptation of the formula yields to

$$I_{AP} = IR^a e^{2bR} / \left((1 - k_s) \cos(\vartheta) + k_s \cos^n(2\vartheta) \right) \quad (8)$$

with the specular reflectance parameter k_s and the degree of the specular reflectance n , which can be iterative optimized within a homogenous region.

2.4 Surface orientation

The orientation of the illuminated surface has to be known to accomplish the radiometric calibration of the intensity. For each measured point in the data set all points in a small spherical neighborhood are considered to calculate the covariance matrix and the corresponding eigenvalue and eigenvector (Gross & Thoennessen, 2006). With the determined eigenvalues plane surface areas can be segmented and the orientation of the surface can be estimated. To decide, whether a point belongs to a planar surface or not, the planarity $p = (\lambda_2 - \lambda_3) / \lambda_1$ based on descend-sorted eigenvalues of the covariance matrix (West et al., 2004) is used.

3. DATA SET

A measurement campaign was carried out to investigate the influences of the incidence angle on the measured intensity. For the scene an urban area including buildings, streets, grassland, and trees was selected. The data was gathered with the RIEGL LMS-Q560. Several flights with different trajectories to gain overlapping stripes were performed. The entire scene is covered by a high point density of about 13 points per square meter. Six flight paths are parallel flight path seven crosses the other.

3.1 Point density

The calculation of the incidence angle and the planarity is based on the determination of the covariance for each point by including all neighbour points inside a sphere with predefined radius. For a radius of 1m the average of 30.5 points are considered for calculation, if all flight paths are included. For comparison the flight 3 delivers as average only 8.8 points. Increasing the radius by factor 2 the average value of 120.6 points per sphere is given if all flight paths considered where 33.6 points are originated from flight 3.

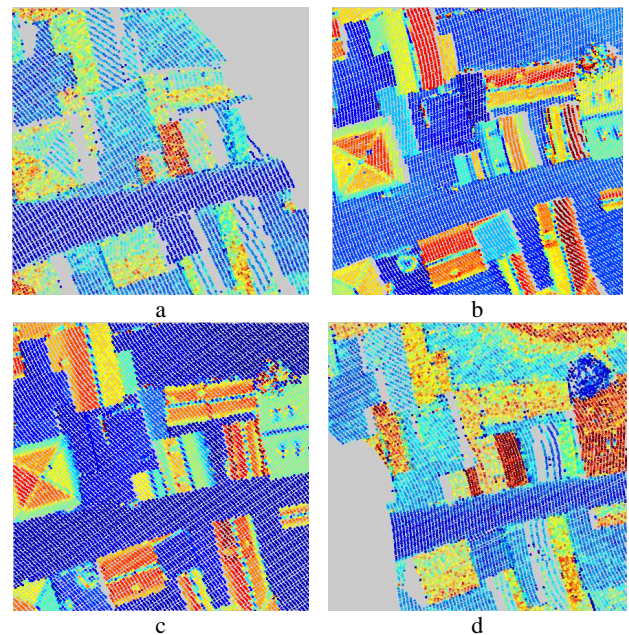


Figure 2. Influence of the incidence angles on the intensity: a) flight path 2, b) flight path 3, c) flight path 4, d) flight path 5.

3.2 Influence of the flight paths on the incidence angle

The influences of the flight path respectively the local incidence angle on the intensity values is shown in Figure 2. The trajectories 2 to 5 have about 330m distance. Already a small offset (116m) between the two flight path trajectories 2 and 3, yields essential different incidence angles like presented in Figure 2a and b. The square building with four roof planes on the left border of the image (Figure 2a-c) demonstrates, that small angles are given, if the plane normal vectors point to the sensor. Larger ones can be observed, if the normal vector is orientated to the opposite direction. The point cloud of Flight 2 (Figure 2a) covers mainly the west side of the roof planes (saddle roof) from the buildings in the centre of the image. The measured intensity values of roof planes pointing to the west direction are significant higher than the roof planes pointing to the east direction. The flight 5 (Figure 2d) shows a vice-versa situation.

4. SELECTION OF HOMOGENEOUS REGIONS

For the assessment of the adapted intensity I regions with different orientations but homogenous surface reflectance are used to separate the influences of the incidence angle and material effects. The roof planes within the scene cover a large variety of possible incidence angles but most of them have same tiles. The selected regions contain the same material but varying angle vs. flight direction and the direction of the laser beam. Each roof plane is labelled by a region number.

This selection includes a wide range concerning the off nadir angle for the laser beam. The variation inside the regions is small because the regions are small in comparison with the distance to the sensor. The slope angle of the roof planes (Figure 3a) encloses a few nearly flat roofs but also steeper roofs up to 50°. For each point of the point cloud inside the region the slope angle is calculated based on the eigenvector of the smallest eigenvalue. Therefore the data set encloses regions with small and height variations of the slope angle, which may be influenced by small objects on top of the roofs.

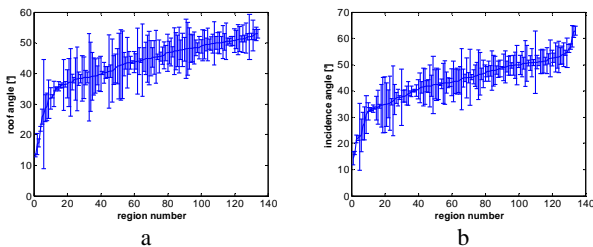


Figure 3. Angles [°] of flight 3 for all selected plane regions sorted by the mean angle together with its standard deviation: a) slope of roofs, b) incidence angles.

The planarity yields high values for plane objects, where the mean value varies from 0.67 to 0.83. Due to noise and disturbing small object parts, higher values could not be achieved. The standard deviation inside the regions varies from 0.06 to 0.13, which indicates, that the planes are not exactly planar and do not show the same roughness. This could be refined by utilizing RANSAC to decrease the number of outliers which have a negative influence on the planarity. The incidence angle (Figure 3b) varies from 2° to 68° with a mean value from 44°. The standard deviation delivers values from 0.5° to 12° with a mean value from 4°. Inside a region the variation of the incidence angle for single flights is small. The distances R between sensor and object surface varies from 429m to 449m with a mean standard deviation of 1m.

5. RESULTS

5.1 Parameter estimation for the investigated data set

Without any prior knowledge for the selected regions the general optimal solution of the linear system of equations is shown in Table 1 (upper row) and with presetting the exponent of the divergence to $a = 2$ the parameter estimation is given in Table 3 (lower row). The estimated extinction parameter $b = 0.00022[1/m]$ is equal to the attenuation of $0.95[dB/km]$, which is given for *clear* weather condition (Jelalian, 1992). The atmospheric attenuation versus wavelength (0.7 to 10.6µm) for lasers is within the range of $0.2[dB/km]$ for extremely clear weather conditions up to $9[dB/km]$ for *light fog* or *rain*.

| divergence | a | b | c | d |
|------------|------|---------|-------|--------|
| unknown | 2.08 | 0.00012 | -0.60 | -21.42 |
| a = 2 | 2.00 | 0.00022 | -0.60 | -20.98 |

Table 1. Results of the parameter estimation.

5.2 Normalization results for the regions

For the selected regions the given intensity is normalized by the optimized cosine exponent (reflectance adaptation parameter c) and the division with the cosine of the incidence angle ϑ . By this division the normalized intensity value increases compared to the original one. Therefore the mean value $\mu(x)$ and the standard deviation $\sigma(x)$ is used for the calculation of the variation parameter $V_c(x) = \sigma(x)/\mu(x)$. This parameter is scale invariant and regards the dependency of the standard deviation from the intensity as presented by Pfeifer et al. (2007).

Mean value and standard deviation of the variation parameter over all roof regions with nearly the same material

$$\mu(V_c(\text{region})) \text{ and } \sigma(V_c(\text{region}))$$

are determined and presented in Table 2. Considering only flight 3 or 4 there are no significant value modifications, but including flight 3 and 4 together the normalization delivers an essentially smaller standard deviation. The variance of the incidence angle for each region increases, if data from more than one flight are used. In the last column of Table 2 the corresponding values by regarding all flights are given. In this case a good improvement for normalization considering the Lambertian model combined with the optimized cosine exponent (cf. Table 1: $c = -0.60$) is reached.

| Flight paths | 3 | 4 | 3-4 | 1-7 |
|--|-------|-------|-------|-------|
| Original data | | | | |
| $\mu(V_c)$ | 0.151 | 0.147 | 0.179 | 0.223 |
| $\sigma(V_c)$ | 0.029 | 0.027 | 0.040 | 0.034 |
| Normalization considering Lambertian model | | | | |
| $\mu(V_c)$ | 0.150 | 0.149 | 0.152 | 0.158 |
| $\sigma(V_c)$ | 0.027 | 0.025 | 0.024 | 0.024 |

Table 2. Mean value and standard deviation for different flight paths without and with normalization.

For an assessment the ratio of the variation parameter $R_V(\text{region}) = V_{c,after}(\text{region})/V_{c,before}(\text{region})$ for all selected regions after vs. regions before normalization are calculated. If

the ratio is smaller than 1 the intensity could be improved. The sorted ratios are drawn in Figure 4.

Considering the exponent $c = -1$ of the Lambertian model for the cosine of the incidence angle the result could be improved (Figure 4, dotted red). A slightly better result is derived by the consideration of the extinction parameter $b = 0.00022[1/m]$ and the reflectance adaptation parameter $c = -0.60$ (Figure 4, solid green). It has to be mentioned that only in a few cases the values are larger than 1.0, this might be the regions contain chimney and dormer windows. On the other side an uncertainty about the region borders within the homogeneous area is still given.

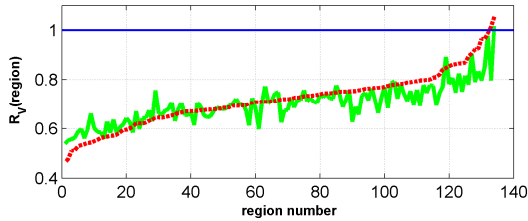


Figure 4. Sorted ratios of the variation parameters before vs. after normalization of the intensity:
 a) normalization by Lambertian model with $c = -1$ (dotted red),
 b) normalization by Lambertian model and reflectance adaptation $c = -0.60$ (solid green).

5.3 Intensity of a region with different geometry

For the investigation on the intensity within a region, two neighbored planes with the same material and the same gradient direction but varying roof slopes are selected. The intensity values for all points inside this region are visualized in Figure 5 coloured by the corresponding flight number. Figure 5a shows the original data and the approximating cosine curve as black line. In Figure 5b the normalized intensity values are scaled in such a way, that the mean value, drawn by a black line, remains the same as before. There exist no points from the flights 1 and 6.

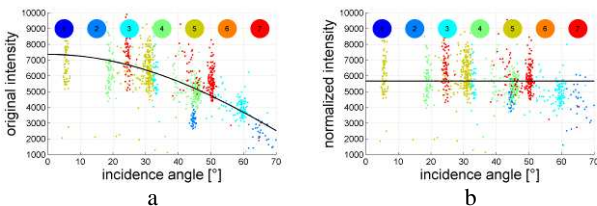


Figure 5. Intensity values vs. incidence angle coloured by the flight number: a) original, b) normalized by Lambertian model with optimized cosine exponent.

Based on the high variation of the intensity before and after normalization by the cosine, it has to be mentioned, that the influence of surface effects like the local unavailable type of material or immeasurable geometry can not be ignored for man-made surfaces. These results imply that the normalized intensity only might be not a sufficient feature for segmentation tasks.

5.4 Parameter estimation based on the Phong model

The above mentioned sub-sections show that an improvement on the intensity could be gained by using the Lambertian surface model with optimized parameters. Due to the additional specular reflectance parameter k_s and the degree of the specular reflectance n which are relevant for the Phong model

the optimization procedure has to be extended to estimate the optimal parameters. In Figure 6 for two selected planes the ratio $R(region) = V_{c,Lambert}(region) / V_{c,Phong}(region)$ of the variation coefficients for Lambert to Phong model is depicted. The solid plane with $R(region) = 1$ is the reference result (Lambertian model), and the gridded plane shows for various combinations of n vs. k_s the performance by using the Phong model.

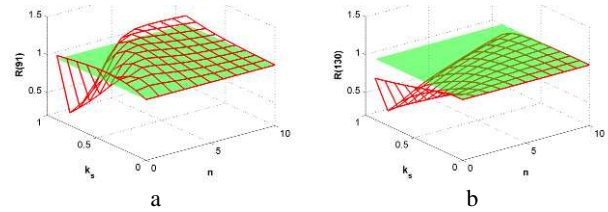


Figure 6. Ratio of the variation parameters adapted by the Lambertian model (solid plane) and the Phong model (gridded plane):
 a) with some small improvements,
 b) without improvements using the Phong model.

The dependency of the backscattered intensity from the incidence angle is shown by Figure 7 for the Lambert and the Phong model with the parameters $k_s = 0.6$ and $n = 4$ under the assumption that both models backscatter the same power. For small incidence angles the Phong model delivers higher intensity values than the Lambert model and lower values for greater incidence angles.

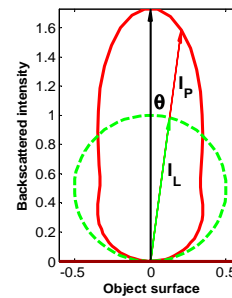


Figure 7. Backscattered intensity for the Lambertian (dotted green) and the Phong (solid red) model dependent on the incidence angle.

For the investigated planes only small improvements could be observed, this might depend on the scattering characteristic of the surface. In addition to this the maximum of the ratio is not very crucial, and then the estimated parameters are not very reliable.

Due to the lack of only one available small data set with limited surfaces only a single material with different orientations could be investigated. The result derived by this data set using the Lambertian model, which is a part of the Phong model, seems to be sufficient.

5.5 Visualization of the normalized intensity data

The intensity improvements are demonstrated by the following figures showing the intensity values before and after the normalization by the incidence angle. For comparison reasons the colours dark blue and dark red are bounded to the thresholds 5% respectively 95% as lower and upper percentiles of the intensity. The normalized intensity reflects higher intensities without large variations for the roof planes but lower values for points near the ridge, where the planarity is not given.

The original data and the corresponding results are shown in Figure 8. A building composed by several parts (mainly gabled roofs) with different orientation is given in Figure 8a. The original data demonstrates the dependency of the intensity from the incidence angle. By the normalization of the intensity this dependency is almost compensated. In Figure 8c the original data with a pyramidal roof shows higher values for the south-west orientated planes than for the north-east ones caused by the flight paths and directions. In the normalized data all four planes have same intensity values and appear homogeneous.

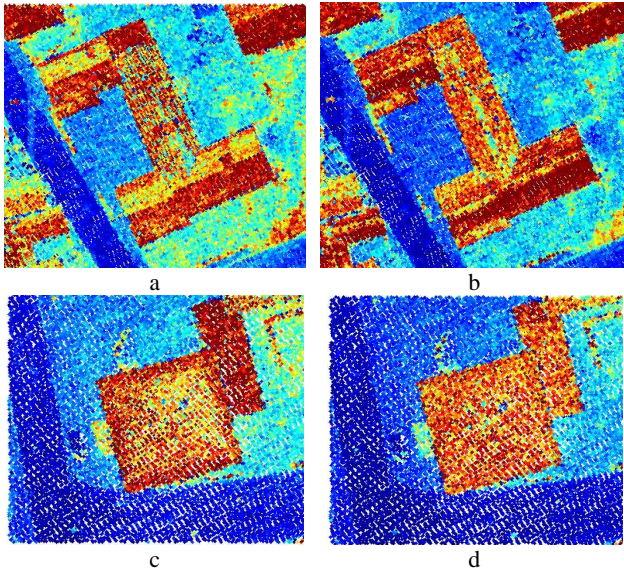


Figure 8. Intensity data for different orientated roofs: gabled roofs: a) original, b) normalized, pyramidal roof: c) original, d) normalized.

6. DISCUSSION AND CONCLUSION

For assessing the normalized intensity values nearly homogenous regions have been selected interactively. The variation parameter is selected as measure for the comparison of the values before and after normalization. Mean and standard deviation of this measure over all regions decreases by the normalization, especially if all flights are included. For pulsed laser systems a strong intensity variation could be observed. The intensity inside a region shows a high variance even for a constant incidence angle. This may be caused by material features or local surface effects.

For nearly all regions the results for the intensity have been improved, even with region disturbances on the roofs like chimneys. The Lambertian model fits the investigated surfaces well. For specular reflectance based on the Phong model no significant improvements could be derived. This might depend on the diffuse backscattering characteristic of the material. Further investigations for this study were not possible because only one data set with surfaces of a single material with different orientations was available. For terrestrial laser data enhanced results can be expected, with a lower variance of the intensity, due to a better signal-to-noise ratio for the measured data.

This paper proposes a general approach for intensity normalization considering diffuse and specular scattering characteristics of the surface. This assumption should be proved in future by investigating reference targets where the backscattering characteristic is known or could be measured by reference measurements.

REFERENCES

- Brenner, C., Haala, N., Fritsch, D., 2001. Towards fully automated 3D city model generation. In: Baltsavias, E., Grün, A., van Gool, L. (Eds.) Proceedings of the 3rd International Workshop on Automatic Extraction of Man-Made Objects from Aerial and Space Images, pp. 47-56.
- Briese, C., Höfle, B., Lehner, H., Wagner, W., Pfennigbauer, M., Ullrich, A., 2008. Calibration of full-waveform airborne laser scanning data for object classification. In: Turner, M.D., Kamerman, G.W. (Eds.) Laser Radar Technology and Applications XIII, SPIE Proceedings Vol. 6950, pp. 69500H.
- Geibel, R., Stilla, U., 2000. Segmentation of Laser-altimeter data for building reconstruction: Comparison of different procedures. International Archives of Photogrammetry and Remote Sensing 33 (Part B3), pp. 326-334.
- Gross, H., Thoennessen, U., 2006. Extraction of Lines from Laser Point Clouds. In: Förstner, W., Steffen, R. (Eds.) Symposium of ISPRS Commission III: Photogrammetric Computer Vision PCV06. International Archives of Photogrammetry, Remote Sensing and Spatial Information Sciences 36 (Part 3), pp. 86-91.
- Höfle, B., Pfeifer, N., 2007. Correction of laser scanning intensity data: Data and model-driven approaches. ISPRS Journal of Photogrammetry and Remote Sensing 62 (6), pp. 415-433.
- Hofton, M.A., Minster, J.B., Blair, J.B., 2000. Decomposition of laser altimeter waveforms. IEEE Transactions on Geoscience and Remote Sensing 38 (4), pp. 1989-1996.
- Jelalian, A.W., 1992. Laser Radar Systems. Artech House, Boston, MA.
- Jutzi, B., Stilla, U., 2006. Range determination with waveform recording laser systems using a Wiener Filter. ISPRS Journal of Photogrammetry and Remote Sensing 61 (2), pp. 95-107.
- Kamermann, G.W., 1993. Laser Radar. In: Fox, C.S. (Ed.) Active Electro-Optical Systems, The Infrared & Electro-Optical Systems Handbook. SPIE Optical Engineering Press, Michigan.
- Kaasalainen, S., Hyypä, J., Litkey, P., Hyyppä, H., Ahokas, E., Kukko, A., Kaartinen, H., 2007. Radiometric calibration of ALS intensity. In: Rönnholm, P., Hyyppä, H., Hyypä, J. (Eds.) Laserscanning 2007. International Archives of Photogrammetry, Remote Sensing, and Spatial Information Sciences 36 (Part 3-W52), pp. 201-205.
- Katzenbeisser, R., 2003. Technical Note on Echo Detection. www.toposys.de/pdfext/Engl/echo-detec3.pdf (Accessed 1. Feb. 2008).
- Kukko A., Kaasalainen S., Litkey P., 2007. Effect of incidence angle on laser scanner intensity and surface data. Applied Optics, Vol. 47, No. 7, March 2008, pp. 986-992
- Persson, Å., Söderman, U., Töpel, J., Ahlberg, S., 2005. Visualization and Analysis of Full-Waveform Airborne Laser Scanner Data. In: Vosselman, G., Brenner, C. (Eds.) Laserscanning 2005. International Archives of Photogrammetry, Remote Sensing and Spatial Information Sciences 36 (Part 3/W19), pp. 109-114.
- Pfeifer, N., Dorninger, P., Haring, A., Fan, H., 2007. Investigating terrestrial laser scanning intensity data: quality and functional relations. In: Gruen, A., Kahmen, H. (Eds.) International Conference on Optical 3-D Measurement Techniques VIII, Zürich, Switzerland, ISBN 3-906467-67-8, pp. 328-337.
- Phong, B.T., 1975. Illumination for computer generated pictures. Communications of the ACM 18 (6), pp. 311-317.
- Reshetuyk, Y., 2006. Investigation of the Influence of Surface Reflectance on the Measurements with the Terrestrial Laser Scanner Leica HDS 3000. Zeitschrift für Geodäsie, Geoinformation und Landmanagement 131 (2), pp. 96-103.
- Shan, J., Toth, C.K., (Eds.) 2008. Topographic Laser Ranging and Scanning: Principles and Processing. Boca Raton, FL: Taylor & Francis.
- Wagner, W., Hyypä, J., Ullrich, A., Lehner, H., Briese, C., Kaasalainen, S., 2008. Radiometric Calibration of Full-Waveform Small-Footprint Airborne Laser Scanners. International Archives of Photogrammetry, Remote Sensing and Spatial Geoinformation Sciences 37(B1), pp.163-168.
- Wagner, W., Ullrich, A., Ducic, V., Melzer, T., Studnicka, N., 2006. Gaussian Decomposition and Calibration of a Novel Small-Footprint Full-Waveform Digitising Airborne Laser Scanner. ISPRS Journal of Photogrammetry and Remote Sensing, 60 (2), pp. 100-112.
- West, K.F., Webb, B.N., Lersch, J.R., Pothier, S., Triscari, J.M., Iverson, A.E., 2004. Context-driven automated target detection in 3d data. In: Sadjadi, F.A. (Ed.) Automatic Target Recognition XIV. Proceedings of SPIE Vol. 5426, pp. 133-143.